A Lagrangian Fibration of the Isotropic 3-Dimensional Harmonic Oscillator with Monodromy

Chiscop, I.; Dullin, H. R.; Efstathiou, K.; Waalkens, H.

Published in:
Journal of Mathematical Physics

DOI:
10.1063/1.5053887

Publication date:
2019

A Lagrangian fibration of the isotropic 3-dimensional harmonic oscillator with monodromy

Cite as: J. Math. Phys. **60**, 032103 (2019); https://doi.org/10.1063/1.5053887
Submitted: 27 August 2018 . Accepted: 06 March 2019 . Published Online: 25 March 2019

Irina Chiscop, Holger R. Dullin, Konstantinos Efstathiou, and Holger Waalkens

Journal of Mathematical Physics ARTICLE scitation.org/journal/jmp

A Lagrangian fibration of the isotropic 3-dimensional harmonic oscillator with monodromy

Cite as: J. Math. Phys. 60, 032103 (2019); doi: 10.1063/1.5053887
Submitted: 27 August 2018 • Accepted: 6 March 2019 •
Published Online: 25 March 2019

Irina Chiscop,[1] Holger R. Dullin,[2] Konstantinos Efstathiou,[1] and Holger Waalkens[1]

AFFILIATIONS

[1] Bernoulli Institute for Mathematics, Computer Science and Artificial Intelligence, University of Groningen, Groningen, The Netherlands
[2] School of Mathematics and Statistics, University of Sydney, Sydney, Australia

ABSTRACT

The isotropic harmonic oscillator in dimension 3 separates in several different coordinate systems. Separating in a particular coordinate system defines a system of three Poisson commuting integrals and, correspondingly, three commuting operators, one of which is the Hamiltonian. We show that the Lagrangian fibration defined by the Hamiltonian, the z component of the angular momentum, and a quartic integral obtained from separation in prolate spheroidal coordinates has a non-degenerate focus-focus point, and hence, non-trivial Hamiltonian monodromy for sufficiently large energies. The joint spectrum defined by the corresponding commuting quantum operators has non-trivial quantum monodromy implying that one cannot globally assign quantum numbers to the joint spectrum.

I. INTRODUCTION

The isotropic harmonic oscillator is at the same time the simplest and one of the most important systems in physics. The system is very special in both the classical and the quantum setting. All solutions of the classical equations of motion are periodic and even have the same period. The quantum system is special in that it has an equidistant energy spectrum. The best explanation of these special properties in both the classical and the quantum setting is the high SU(3) symmetry of the system (see Ref. 1) which makes the system super-integrable.

A classical *integrable Hamiltonian system* (IHS) in N degrees of freedom has exactly N independent and mutually Poisson commuting integrals with one of them being the Hamilton function. The joint level sets of the integrals define a *Lagrangian fibration* of phase space by N-dimensional tori. The local geometry of the fibration is given by the Liouville-Arnold Theorem[2] which also ensures the local existence of classical actions. Passing to the quantum setting, a *quantum integrable system* (QIS) is a set of N commuting operators $\mathcal{H} = (\hat{H}_1, \ldots, \hat{H}_N)$ with, say, $\hat{H}_1$ being the Hamilton operator of the system. Because the operators commute, their spectra can be measured simultaneously, $\hat{H}_i\psi = \lambda_i\psi$, $i = 1, \ldots, N$. Together, they define the joint spectrum which associates a point in $N-$dimensional space with coordinates λ_i to each joint eigenfunction ψ. It follows from the Bohr-Sommerfeld quantization of classical actions that the joint spectrum locally has the structure of a lattice $\mathbb{Z}^N$.

A classical *super-integrable* system in N degrees of freedom is one that has more than N independent integrals. The classical geometry of super-integrable systems is well understood.[3] Fixing the values of the integrals defines tori of lower dimension than in the Liouville-Arnold Theorem, and Nekhoroshev showed that one can construct lower dimensional action-angle coordinates in a kind of generalization of the Liouville-Arnold Theorem.[4] More global aspects have been studied in Refs. 5 and 6. Given a super-integrable system with more than N integrals, one can choose N of them, including the Hamiltonian, to define an IHS or, equivalently, a Lagrangian fibration of phase space. Such choices of N integrals can define non-equivalent Lagrangian fibrations. Reflecting the classical setting, if a Hamiltonian $\hat{H}$ is super-integrable, then there are distinct QISs determined by a specific choice of N commuting operators that share the given Hamiltonian $\hat{H}$, but form non-equivalent QISs with in general different joint spectra. The eigenvalues of $\hat{H}$ and their degeneracy are the same in each realisation, but the

joint spectrum within a degenerate eigenspace and the corresponding basis of eigenfunctions are different. From the classical geometric point of view, considering tori with half the dimension of phase space in a super-integrable system appears somewhat arbitrary. However, from the quantum point of view, it is prudent to study all possible sets of commuting observables because these tell us what can be measured simultaneously as the uncertainty principle is trivial in this case.

In this paper, we are focusing on the case where the different IHSs or corresponding QISs are obtained from separation in different coordinate systems. Separation in different coordinate systems gives different IHSs with the same Hamilton function H or QISs with the same Hamilton operator $\hat{H}$. A Hamiltonian that is multi-separable is also super-integrable since there are more than N integrals. Schwarzschild[7] was the first to point out that if the Hamilton-Jacobi equation of H can be separated in more than one coordinate system, the quantum energy eigenvalues of $\hat{H}$ are degenerate. Such a Hamiltonian operator $\hat{H}$ is called multi-separable and is hence included in non-equivalent QIS's $\mathcal{H}$ and $\mathcal{G}$. The simplest multi-separable systems are the free particle, the Kepler problem, and the harmonic oscillator. A multi-separable system with N degrees of freedom is super-integrable because if both $\mathcal{H}$ and $\mathcal{G}$ contain $\hat{H}$, then we have found more than $N-1$ operators that commute with $\hat{H}$. An important group of 3-dimensional super-integrable and multi-separable systems is classified in Ref. 8.

The isotropic three-dimensional harmonic oscillator is maximally super-integrable which means that, together with the Hamiltonian, it has five independent integrals. The joint level sets are one-dimensional tori, i.e., periodic orbits, whose projection to configuration space are ellipses centered at the center of the force. Super-integrability manifests itself in the degeneracy of the quantum energy spectrum: the total number of states of a three-dimensional harmonic oscillator with angular frequency ω and energy $E = \hbar\omega(n + 3/2)$ is $(n + 1)(n + 2)/2$ with the "principal" quantum number $n = 0, 1, 2, \ldots$ (see Ref. 9).

It is also well known that the isotropic 3-dimensional harmonic oscillator is multi-separable. On one hand, it separates in Cartesian coordinates into a sum of one-degree-of-freedom harmonic oscillators so that the wave function for the multi-dimensional case is simply a product of wave functions for the one-dimensional case, which are given in terms of Hermite polynomials. On the other hand, it separates in spherical coordinates, which leads to wave functions that are products of spherical harmonics and associated Laguerre polynomials. In the first case, we have a quantum number $n_i = 0, 1, 2, \ldots$ for each 1D oscillator, and the eigenvalues of $\hat{H}$ are $E = \hbar\omega(n + 3/2) = \hbar\omega(n_1 + n_2 + n_3 + 3/2)$. In the second case (see, e.g., Ref. 10), we have $E = \hbar\omega(2k + l + 3/2)$ for the non-negative integer k where l is the total angular momentum eigenvalue with $l = n, n-2, n-4, \ldots$ down to 0 or 1, depending on whether n is even or odd, respectively. In addition, there is the usual "magnetic" quantum number $m = -l, \ldots, l$. In both cases, the quantum states form a lattice in which lattice points can be uniquely labelled by quantum numbers. The details of the two lattices are, however, different. In particular, the actions are not even locally related by unimodular transformation like in the case of integrable systems.

In this work, we consider the separation of the isotropic harmonic oscillator in *prolate spheroidal coordinates*. Prolate spheroidal coordinates are a family of coordinate systems where the family parameter a is half the distance between the focus points of a family of confocal ellipses and hyperbolas, which in order to get corresponding coordinate surfaces are rotated about the axis containing the focus points. In the limit $a \to 0$, spherical coordinates are obtained, and in the limit $a \to \infty$, parabolic coordinates are obtained. The separation leads to three integrals: the harmonic oscillator Hamiltonian H, the z-component L_z of angular momentum, and a quartic integral G arising from the separation procedure.

Our main result is that the Lagrangian fibration defined by the integrals obtained from separating the harmonic oscillator in prolate spheroidal coordinates has *non-trivial Hamiltonian monodromy*[11] when the energy $E > \frac{1}{2}\omega^2 a^2$. Classically, this implies that the Lagrangian fibration cannot be globally described through action-angle variables, while in the quantum context the joint spectrum of $\hat{H}$, $\hat{L}_z$, $\hat{G}$ cannot be assigned three global quantum numbers. Our approach is similar to a recent analysis of the Kepler problem, which through separation in prolate spheroidal coordinates leads to a quantum integrable system that does not possess three global quantum numbers.[12] The latter result had in a sense been anticipated in Ref. 13 where it was shown that the two-center problem, which is separable in prolate spheroidal coordinates, has monodromy.

Monodromy and generalizations of monodromy[14,15] have been extensively studied in recent years and have been found for many different systems; see, e.g., Ref. 16 and the references therein. Quantum monodromy manifests itself as a lattice defect in the joint spectrum that prevents the global assignment of quantum numbers.[17–20] Quantum monodromy explains, e.g., problems in assigning rovibrational spectra of molecules[21–23] or electronic spectra of atoms in external fields.[24,25] Moreover, it provides a mechanism for excited-state quantum phase transitions.[26,27] The generalization of monodromy to scattering systems has been shown to lead to defects in the lattice of transparent states in planar central scattering[28] (see also Refs. 29 and 30 for a more general perspective on monodromy in classical potential scattering). Monodromy can also play a role in spatiotemporal nonlinear wave systems,[31] and dynamical manifestations of monodromy have recently been studied in Ref. 32.

Monodromy is not an intrinsic property of the fibration of the phase space of the isotropic 3-D harmonic oscillator by 1-tori (periodic orbits). It is a property of a specific Lagrangian fibration, a specific arrangement of these 1-tori into 3-tori, induced by the choice of integrals H, L_z, and G arising from separation in prolate spheroidal coordinates. Even though this is only one out of many possible Lagrangian fibrations that can be defined by arranging the 1-tori in different ways, it is also of a more general interest. Consider Hamiltonian systems where the function F is invariant under the oscillator and axial symmetries induced by the flows of H and L_z, respectively. It is then natural to ask which functions F lead to Lagrangian fibrations (defined by H, L_z, and F) with monodromy. Our results imply that $F = G$ has this property. Moreover, the corresponding singular Lagrangian fibration for fixed positive $H = E > 0$ provides a concrete realization of an almost toric system appearing in the classification by Ref. 33. The fibration's base space is a disk D, the total space is $\mathbb{C}P^2$, and there are $n = 1$ focus-focus points (nodes) and $k = 2$ elliptic-elliptic points (vertices); see also Ref. 34.

However, choosing $F = G$ is not the only such example and indeed its significance becomes apparent when it is viewed as a member of a particular family of axially symmetric integrable perturbations of the isotropic 3-D harmonic oscillator. Specifically, consider Hamilton functions that, as before, are invariant under the oscillator and axial symmetries but also Poisson commute with G. A Taylor expansion and truncation to quartic terms of such F gives a Hamilton function $F^{(4)}$ which must be a linear combination of quadratic terms H, L_z and quartic terms HL_z, G. After singular reduction of the symmetries the only non-trivial remaining term is G. Therefore, the Lagrangian fibration defined by $(H, L_z, F^{(4)})$ and the one defined by (H, L_z, G) are equivalent. Moreover, if higher-order terms in the Taylor expansion of F are sufficiently small compared to $F^{(4)}$, monodromy will also be a property of the Lagrangian fibration defined by (H, L_z, F). This shows, in particular, that there exists a family of axially symmetric, integrable, perturbations of H whose Lagrangian fibration possesses monodromy and whose study boils down to the study of the Lagrangian fibration defined by (H, L_z, G) which is the main aim of this work. We note that perturbations of isotropic harmonic oscillators have many applications. Examples where similar techniques as in this paper are used include assigning rovibrational spectra of molecules using polyads,[35] ion traps,[36] and galactic dynamics.[37] It is to be expected that the results of our paper has applications along the same line which deserves further investigation.

This paper is organized as follows: In Sec. II, we introduce the classical three-dimensional isotropic harmonic oscillator and discuss its symmetries and its separation in prolate spheroidal coordinates. In Sec. III, we compute the bifurcation diagram for the energy momentum map associated with separation in prolate spheroidal coordinates and prove the presence of monodromy. The effect of monodromy on the quantum spectrum is studied in Sec. IV. We conclude with some comments in Sec. V.

II. CLASSICAL SEPARATION IN PROLATE SPHEROIDAL COORDINATES

The three-dimensional isotropic harmonic oscillator has the Hamiltonian

$$H = \frac{1}{2}|\mathbf{p}|^2 + \frac{\omega^2}{2}|\mathbf{r}|^2, \tag{1}$$

where $\mathbf{r} = (x,y,z)^T$ and $\mathbf{p} = (p_x, p_y, p_z)^T$ are the canonical variables on the phase space $T^*\mathbb{R}^3 \cong \mathbb{R}^6$. By choosing suitable units, we can assume that the frequency ω has the value 1. But in order to identify terms arising from the potential, we will keep ω in the equations below. Not only are the three separated Hamiltonians

$$\mathbf{A} = \left(\tfrac{1}{2}(p_x^2 + \omega^2 x^2), \tfrac{1}{2}(p_y^2 + \omega^2 y^2), \tfrac{1}{2}(p_z^2 + \omega^2 z^2)\right)^T,$$

constants of motion, but so are the components of the angular momentum $\mathbf{L} = \mathbf{r} \times \mathbf{p}$. Not all these integrals are independent. But any five of them are so that H is maximally super-integrable.

Define

$$\mathbf{B} = \left(\{L_x, A_y\}, \{L_y, A_z\}, \{L_z, A_x\}\right)^T,$$

where $\{\cdot,\cdot\}$ is the Poisson bracket. The algebra of 9 quadratic integrals $\mathbf{A}$, $\mathbf{B}$, $\mathbf{L}$ closes and defines a Lie-Poisson bracket, shown in Table I, that is isomorphic to the Lie algebra $\mathfrak{su}(3)$ (see also Ref. 1). Fixing the relations between the integrals $\mathbf{A}$, $\mathbf{B}$, $\mathbf{L}$ defines an embedding of the reduced symplectic manifold $\mathbb{C}P^2$ into $\mathbb{R}^9$. Here, $\mathbb{C}P^2$ is the orbit space of the S^1 action induced on $\mathbb{C}^3 \simeq T^*\mathbb{R}^3$ by the Hamiltonian flow of H.[38,39] The Hamiltonian $H = A_x + A_y + A_z$ is a Casimir. The algebra has two more Casimirs, the quadratic $C_2 = 2\mathbf{A}^2 + \omega^2\mathbf{L}^2 + \mathbf{B}^2$ and the cubic

$$C_3 = 6\,\mathrm{Re}(w_x w_y w_z) + \sum_{k=x,y,z} 2|w_k|^2(H - 3A_k) - \frac{8}{27}(H - 3A_k)^3,$$

TABLE I. Poisson structure on $\mathbb{C}P^2$.

$\{\downarrow, \rightarrow\}$	A_x	A_y	A_z	L_x	L_y	L_z	B_x	B_y	B_z
A_x	0	0	0	0	B_y	$-B_z$	0	$-\omega^2 L_y$	$\omega^2 L_z$
A_y	0	0	0	$-B_x$	0	B_z	$\omega^2 L_x$	0	$-\omega^2 L_z$
A_z	0	0	0	B_x	$-B_y$	0	$-\omega^2 L_x$	$\omega^2 L_y$	0
L_x	0	B_x	$-B_x$	0	L_z	$-L_y$	$2A_z - 2A_y$	$-B_z$	B_y
L_y	$-B_y$	0	B_y	$-L_z$	0	L_x	B_z	$2A_x - 2A_z$	$-B_x$
L_z	B_z	$-B_z$	0	L_y	$-L_x$	0	$-B_y$	B_x	$2A_y - 2A_x$
B_x	0	$-\omega^2 L_x$	$\omega^2 L_x$	$2A_y - 2A_z$	$-B_z$	B_y	0	$-\omega^2 L_z$	$\omega^2 L_y$
B_y	$\omega^2 L_y$	0	$-\omega^2 L_y$	B_z	$2A_z - 2A_x$	$-B_x$	$\omega^2 L_z$	0	$-\omega^2 L_x$
B_z	$-\omega^2 L_z$	$\omega 2 L_z$	0	$-B_y$	B_x	$2A_x - 2A_y$	$-\omega^2 L_y$	$\omega^2 L_x$	0

where $w_k = B_k + i\omega L_k$, $k = x, y, z$.

The huge symmetry of the isotropic harmonic oscillator is also reflected by its separability in different coordinate systems. In fact, the three-dimensional oscillator separates in several different coordinate systems. The most well known are the systems of Cartesian coordinates and spherical coordinates (see, e.g., Ref. 1). In this paper, we will be studying the separation in prolate spheroidal coordinates. The separability in these coordinates is, e.g., mentioned in Ref. 40. The coordinates are defined with respect to two focus points which we assume to be located on the z axis at $\mathbf{a} = (0, 0, a)$ and $-\mathbf{a} = (0, 0, -a)$ where $a > 0$. The prolate spheroidal coordinates are then defined as

$$(\xi, \eta, \varphi) = \Big(\frac{1}{2a}(r_+ + r_-),\ \frac{1}{2a}(r_+ - r_-),\ \arg(x + \mathrm{i}y)\Big),$$

where $r_\pm = |\mathbf{r} \pm \mathbf{a}|$. They have ranges $\xi \geq 1$, $-1 \leq \eta \leq 1$, and $0 \leq \varphi \leq 2\pi$. The surfaces of constant $\xi > 1$ and $-1 < \eta < 1$ are confocal prolate ellipsoids and two-sheeted hyperboloids which are rotationally symmetric about the z axis and have focus points at $\pm\mathbf{a}$. For $\xi \to 1$, the ellipsoids collapse to the line segment connecting the focus points, and for $\eta \to \pm 1$, the hyperboloids collapse to the half-lines consisting of the part of the z axis above and below the focus points, respectively.

The Hamiltonian in prolate spheroidal coordinates becomes

$$H = \frac{1}{2}\frac{1}{a^2(\xi^2 - \eta^2)}(p_\xi^2(\xi^2 - 1) + p_\eta^2(1 - \eta^2)) + \frac{1}{2}\frac{p_\varphi^2}{a^2(\xi^2 - 1)(1 - \eta^2)} + \frac{1}{2}a^2\omega^2(\xi^2 + \eta^2 - 1).$$

The angle φ is cyclic. So p_φ which is the z component of the angular momentum is a constant of motion. Multiplying the energy equation $H = E$ by $2a^2(\xi^2 - \eta^2)$ and reordering terms gives the separation constant

$$\begin{aligned} G &:= -p_\xi^2(\xi^2 - 1) - \frac{l_z^2}{\xi^2 - 1} - a^4\omega^2\xi^2(\xi^2 - 1) + 2a^2(\xi^2 - 1)E \\ &= p_\eta^2(1 - \eta^2) + \frac{l_z^2}{1 - \eta^2} + a^4\omega^2\eta^2(1 - \eta^2) - 2a^2(1 - \eta^2)E, \end{aligned} \tag{2}$$

where we use l_z to denote the value of p_φ. Rewriting the separation constant in Cartesian coordinates gives

$$G = L_x^2 + L_y^2 + L_z^2 - 2a^2(A_x + A_y). \tag{3}$$

The functions $\mathcal{G} = (H, L_z, G)$ are independent and their mutual Poisson brackets vanish. They thus define a Liouville integrable system which as we will see has a singular foliation by Lagrangian tori with monodromy which we then also study quantum mechanically.

III. BIFURCATION DIAGRAM AND REDUCTION

Solving (2) for the momenta p_η and p_ξ, we get

$$p_\xi^2 = \frac{P(\xi)}{(\xi^2 - 1)^2} \quad \text{and} \quad p_\eta^2 = \frac{P(\eta)}{(\eta^2 - 1)^2}, \tag{4}$$

where

$$P(s) = -l_z^2 + 2a^2(1 - s^2)\Big[\Big(E - \frac{1}{2}a^2\omega^2 s^2\Big)(1 - s^2) + \frac{g}{2a^2}\Big] \tag{5}$$

with g denoting the value of the separation constant G. The roots of the polynomial $P(s)$ are turning points in the corresponding separated degree of freedom, i.e., roots in $[-1, 1]$ correspond to turning points in the (η, p_η) phase plane and roots in $[1, \infty)$ correspond to turning points in the (ξ, p_ξ) phase plane. Critical motion occurs for values of the constants of motion where turning points collide, i.e., for double-roots of $P(s)$. The bifurcation diagram, i.e., the set of critical values of the energy momentum map $\mathcal{G} = (H, L_z, G) : T^*\mathbb{R}^3 \to \mathbb{R}^3$, $(\mathbf{r}, \mathbf{p}) \mapsto (E, l_z, g)$, can thus be found from the vanishing of the discriminant of the polynomial $P(s)$. However, care has to be taken due to the singularities of the prolate spheroidal coordinates at the focus points. In Sec. III C, below we will therefore derive the bifurcation diagram more rigorously using the method of singular reduction.[41] For $l_z = 0$, the motion (in configuration space) takes place in invariant planes of constant angles about the z axis. We will consider this case first and study the case of general l_z afterwards.

A. The two-dimensional harmonic oscillator ($l_z = 0$)

From the one-parameter family of two-dimensional harmonic oscillators with $l_z = 0$, we will consider the one in the (x, z) plane. This is an integrable system with the energy momentum map (H, G) where H and G are the constants of motion defined in (1) and (3) restricted to $y = p_y = 0$. For $l_z = 0$, the roots of $P(s)$ are

$$s_{1\pm} = \pm 1,$$
$$s_{2\pm} = \pm\frac{1}{2\omega a}\sqrt{2a^2\omega^2 + 4h - 2\sqrt{(a^2\omega^2 - 2E)^2 - 4g\omega^2}},$$
$$s_{3\pm} = \pm\frac{1}{2\omega a}\sqrt{2a^2\omega^2 + 4h + 2\sqrt{(a^2\omega^2 - 2E)^2 - 4g\omega^2}}.$$

For values (E, g) for which $s_{2\pm}$ and $s_{3\pm}$ are real, we have $|s_{2\pm}| \le |s_{3\pm}|$. If $s_{3\pm}$ are not real, then $s_{2\pm}$ are also not real. But conversely, $s_{3\pm}$ can be real even if $s_{2\pm}$ are not real. The discriminant of $P(s)$ is

$$\mathrm{discrim}(P(s), s) = 64\, a^{12}\omega^2\left(2\,a^2E + g\right)g^4\left(\left(a^2\omega^2 - 2E\right)^2 - 4\,g\omega^2\right)^2.$$

Double roots occur for

$$\mathcal{L}_1 := \{g = -2\,a^2E\},\ \mathcal{L}_2 := \{g = 0\},\ \mathcal{L}_3 := \{g = \frac{(a^2\omega^2 - 2\,E)^2}{4\,\omega^2}\}.$$

The curves $\mathcal{L}_i$, $i = 1, 2, 3$, divide the upper (g, E) half plane into five region with different dispositions of roots as shown in Fig. 1. From the separated momenta in (4), we see that the values of the constants of motion facilitate physical motion (i.e., real momenta) if the resulting $P(s)$ is positive somewhere in $[-1, 1]$ and at the same time positive somewhere in $[1, \infty)$. From Fig. 1, we see that this is the case only for regions III and IV. For a fixed energy $E \ge 0$, the minimal value of g is determined by the collision of the roots $s_{2\pm}$ at 0, whereas for a fixed energy $E > \frac{1}{2}\omega^2a^2$, the maximal value of g is determined by the collision of the pairs of roots $s_{2\pm}$ and $s_{3\pm}$, and the maximal value of g for a fixed energy $0 < E < \frac{1}{2}\omega^2a^2$ is determined by the collision of the pairs of roots $s_{3\pm}$ and $s_{1\pm} = \pm 1$. At the boundary between regions III and IV, the pairs of roots $s_{2\pm}$ and $s_{1\pm} = \pm 1$ collide.

For a value (E, g) in region IV, the preimage under the energy momentum map (H, G) is a two-torus consisting of a one-parameter family of periodic orbits whose projection to configuration space are ellipses which are enveloped by a caustic formed by the ellipse given by

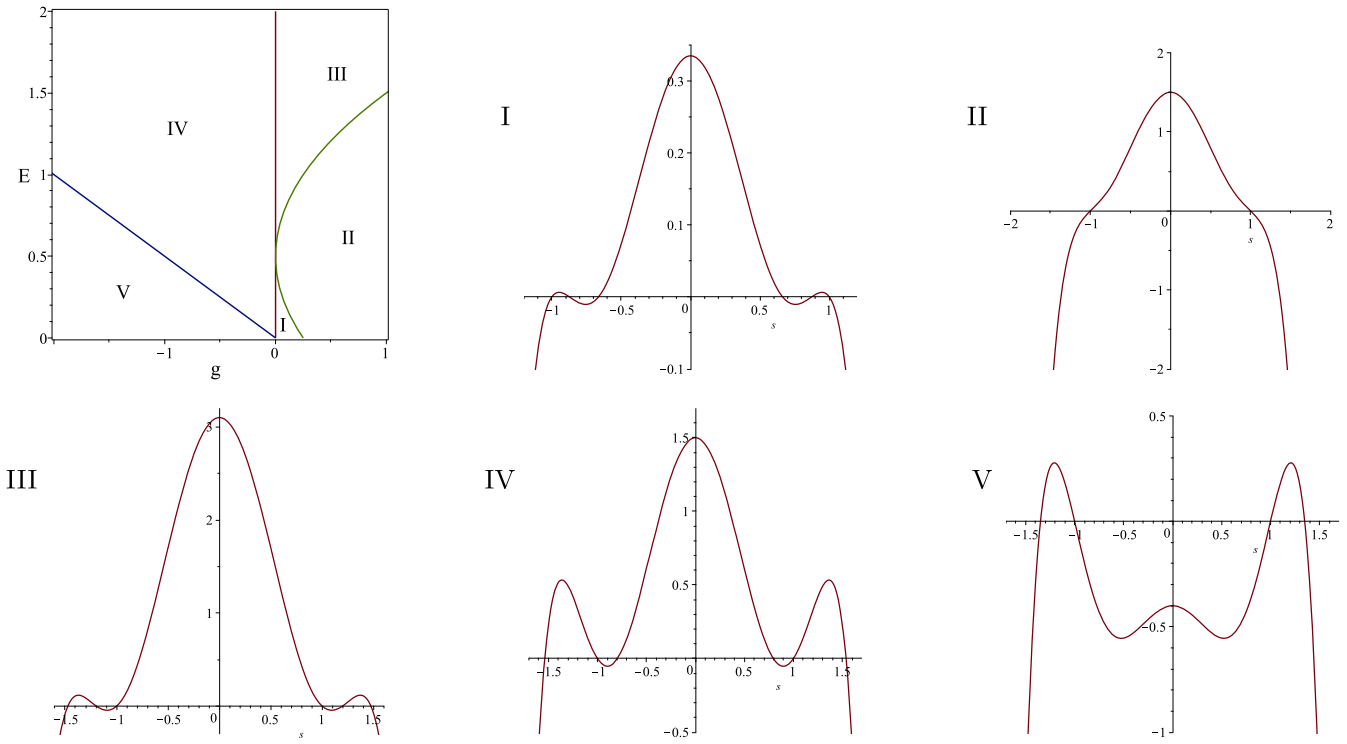

FIG. 1. Bifurcation diagram of the planar harmonic oscillator with energy momentum map (H, G) (top left). The remaining panels show the graphs of the polynomial $P(s)$ for representative values of (E, g) in the regions *I* to *V* marked in the (g, h) plane. In region I, all roots are real and satisfy $|s_{2\pm}| < |s_{3\pm}| < |s_{1\pm}|$. In region II, $s_{2\pm}$ and $s_{3\pm}$ are complex. In region III, all roots are real and satisfy $|s_{1\pm}| < |s_{2\pm}| < |s_{3\pm}|$. In region IV, all roots are real and satisfy $|s_{2\pm}| < |s_{1\pm}| < |s_{3\pm}|$. In region V, $s_{2\pm}$ are complex and $s_{3\pm}$ are real with $|s_{1\pm}| < |s_{3\pm}|$.

the coordinate line $\xi = s_{3+}$ and the two branches of the confocal hyperbola corresponding to the coordinate line $\eta = s_{2+}$ [see Fig. 2(a)]. For a value (E, g) in region III, the preimage under the energy momentum map (H, G) is a two-torus consisting of a one-parameter family of periodic orbits whose projection to configuration space are ellipses which are enveloped by a caustic formed by two confocal ellipses given by the coordinate lines $\xi = s_{2+}$ and $\xi = s_{3+}$, respectively [see Fig. 2(c)]. The boundary $\mathcal{L}_2 = \{g = 0\}$ between regions III and IV is formed by critical values of the energy momentum map (H, G), and the preimage consists of a one-parameter family of periodic orbits whose projection to the configuration space are ellipses which each contain the focus points $\pm\mathbf{a}$ [see Fig. 2(b)]. The family, in particular, contains the periodic orbit oscillating along the z axis with turning points $z_\pm = \pm\sqrt{2E}/\omega$, where $|z_\pm| > a$. The caustic is again formed by the ellipse $\xi = s_{3+}$. For $(E, g) \in \mathcal{L}_2$ and $E < \frac{1}{2}\omega^2 a^2$, the preimage consists only of the periodic orbit oscillating along the z axis between $z_\pm = \pm\sqrt{2E}/\omega$ where $z_\pm$ now has a modulus less than a. For $(E, g) \in \mathcal{L}_3$, i.e., the maximal value of g for fixed energy $E > \frac{1}{2}\omega^2 a^2$, the preimage consists of two periodic orbits whose configuration space projections are the ellipse $\xi = s_{2+} = s_{3+}$. For $(E, g) \in \mathcal{L}_1$, i.e., the minimal value of g for fixed energy E, the preimage consists of the periodic orbit that is oscillating along the x axis with turning points $x_\pm = \pm\sqrt{2E}/\omega$. The tangential intersection of $\mathcal{L}_2$ and $\mathcal{L}_3$ at $(g, E) = (0, \frac{1}{2}\omega^2 a^2)$ corresponds to a pitchfork bifurcation where two ellipse shaped periodic orbits grow out of the periodic orbit along the z axis.

B. The three-dimensional harmonic oscillator (general l_z)

Increasing the modulus of l_z from zero, we see from the definition of $P(s)$ in Eq. (5) that the graphs of the polynomial in Fig. 1 move downward. Even though we cannot easily give expressions for the roots of $P(s)$ for $l_z \neq 0$ we see that increasing $|l_z|$ from zero for fixed E and g, the ranges of admissible η and ξ shrink. Moreover, as $P(\pm 1) = -l_z^2$, the roots stay away from ± 1 (the coordinate singularities of the prolate ellipsoidal coordinates) for $l_z \neq 0$. For general l_z, the discriminant of $P(s)$ is

$$\begin{aligned}\operatorname{discrim}(P(s), s) = 64\, a^{12}\omega^2\big(2\,a^2E + g - l_z^2\big)\big(4\,a^8 l_z^2\,\omega^6 - 24\,a^6 E l_z^2\,\omega^4 - a^4 g^2\omega^4 - 18\,a^4 g l_z^2\,\omega^4 + \\ 27\,a^4 {l_z}^4\omega^4 + 48\,a^4E^2 l_z^2\,\omega^2 + 4\,a^2 g^2 E\omega^2 + 36\,a^2 g E l_z^2\,\omega^2 - 32\,a^2E^3 l_z^2 + 4\,g^3\omega^2 - 4\,g^2E^2\big)^2.\end{aligned}$$

The first (nonconstant) factor vanishes for

$$g = {l_z}^2 - 2\,a^2E. \tag{6}$$

From $P(0) = g - l_z^2 + 2\,a^2E$, we see that this is the condition for the local maximum of $P(s)$ at $s = 0$ to have the value zero or equivalently the collision of roots at 0. In order to see when the second nonconstant factor vanishes it is useful to write $P(s)$ as $(s - d)^2(a_4 s^4 + a_3 s^3 a_2 s^2 + a_1 s + a_0)$, where d is the position of the double root. Comparing coefficients then gives

$$g(d) = -a^2\big(d^2 - 1\big)\big(a^2\omega^2(3d^2 - 1) - 4\,E\big), \tag{7}$$

$$l_z^2(d) = \quad a^2\big(d^2 - 1\big)^2\big(a^2\omega^2(2d^2 - 1) - 2\,E\big). \tag{8}$$

For fixed E and l_z, the minimal value of g is, similarly to the planar case ($l_z = 0$), determined by the occurrence of a double root of $P(s)$ at 0, i.e., by Eq. (6). The maximal value of g for fixed E and l_z is similarly to the planar case determined by the collision of the two biggest roots of $P(s)$ and given by $g(d)$ in Eq. (7) for the corresponding $d > 1$. We present the bifurcation diagram as slices of constant energy for representative values of E. We have to distinguish between the two cases $0 < E < \frac{1}{2}\omega^2 a^2$ and $E > \frac{1}{2}\omega^2 a^2$ as shown in Fig. 3. The upper branches of the bifurcation diagrams in Fig. 3 result from $d > 1$ in Eqs. (7) and (8). A kink at $l_z = 0$ occurs when $E < \frac{1}{2}\omega^2 a^2$. This is because the second factor in

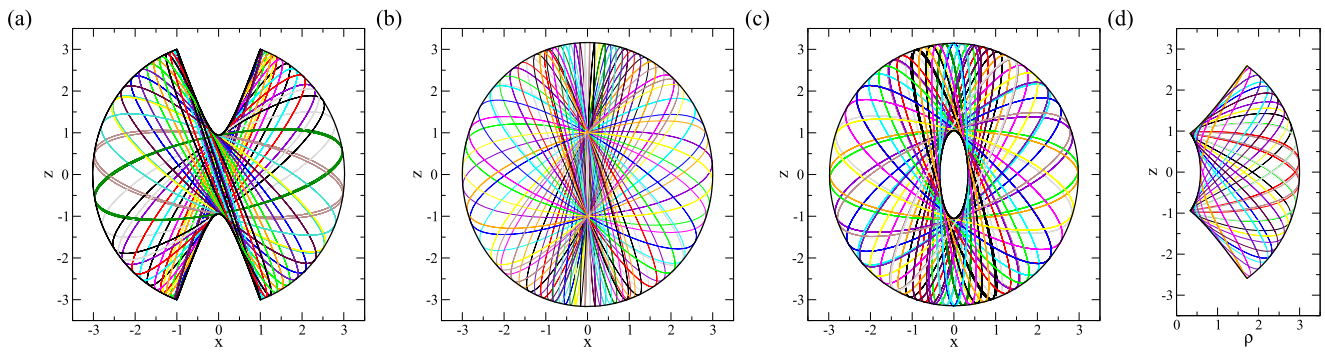

FIG. 2. Orbits and caustics for $h = 5$, $l_z = 0$ and $g = -1$ (region IV) in (a), $g = 0$ (boundary III/IV) in (b) and $g = 1$ (region III) in (c), and $h = 5$, $l_z = 1$ and $g = 0$ in (d), where $\rho = \sqrt{x^2 + y^2}$. In all panels, $a = 1$.

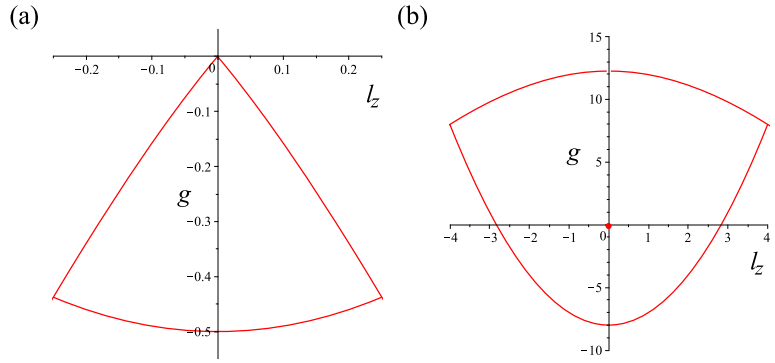

FIG. 3. Slices of constant energy through the spatial bifurcation diagram with $a = 1$, $\omega = 1$ and energies $E = 1/4$ (a) and $E = 4$ (b).

(8) can be zero at a $d \geq 1$ only if $E > \frac{1}{2}\omega^2 a^2$ in which case there is no kink. For $E < \frac{1}{2}\omega^2 a^2$, there is an isolated point at $(l_z, g) = (0, 0)$. This results from $d = \pm 1$ in Eqs. (7) and (8). The point is isolated because the second factor in (8) is negative for $E > \frac{1}{2}\omega^2 a^2$ and $d = \pm 1$. The preimage of a regular value of (H, L_z, G) in the region enclosed by the outer lines bifurcation diagrams in Fig. 3 corresponds to a three-torus formed by a two-parameter family of periodic orbits given by ellipses in configuration space which are enveloped by two-sheeted hyperboloids and two ellipsoids given by coordinate surfaces of the prolate spheroidal coordinates η and ξ, respectively [see Fig. 2(d)]. The preimage of a critical value (E, l_z, g) in the upper branches in Fig. 3 is a two-dimensional torus consisting of periodic orbits that move on ellipsoids of constant ξ. The preimage of a critical value (E, l_z, g) in the lower branches consists of a two-dimensional torus formed by periodic orbits whose projections to configuration space are contained in the (x, y) plane. At the corners where $|l_z|$ reaches its maximal value E/ω, the motion is along the circle of radius $(|l_z|/\omega)^{1/2}$ in the (x, y) plane with the sense of rotation being determined by the sign of l_z.

For the planar case, we saw that the critical energy $E = \frac{1}{2}\omega^2 a^2$ corresponds to a pitchfork bifurcation. In the spatial case, this becomes a Hamiltonian Hopf bifurcation which manifests itself as the vanishing of the kink and detachment of the isolated point in the bifurcation diagram when E crosses the value $\frac{1}{2}\omega^2 a^2$. Note that the critical energy is the potential energy at the focus points of the prolate spheroidal coordinates.

C. Reduction

The isolated point of the bifurcation diagram for energies $E > \frac{1}{2}\omega^2 a^2$ leads to monodromy of the Lagrangian fibration defined by (L_z, G). To see this more rigorously, we proceed as follows: For a classical maximally super-integrable Hamiltonian with compact energy surface, the flow of the Hamiltonian is periodic. Therefore, it is natural to consider symplectic reduction by the S^1 symmetry induced by the Hamiltonian flow. This leads to a reduced system on a compact symplectic manifold. On the reduced space which turns out to be $\mathbb{C}P^2$, we then have a two-degree-of-freedom Liouville integrable system (L_z, G). We will prove that for $E > \frac{1}{2}\omega^2 a^2$, this system has monodromy by showing the existence of a singular fibre with value $(l_z, g) = (0, 0)$ (the isolated point discussed in Subsection III B) given by a 2-torus that is pinched at a focus-focus singular point. To this end, it is useful to also reduce the S^1 action corresponding to the flow of L_z. As this S^1 action has isotropy, standard symplectic reduction is not applicable and we resort to singular reduction using the method of invariants instead. The result will be a one-degree-freedom system on a singular phase space; see Ref. 42 (and also Ref. 43) for a detailed discussion of the singular reduction of these symmetries. For a general introduction to singular reduction, we refer to Refs. 41 and 44, and for the singular reduction of the Keplerian and axial symmetries, which shares similarities to the present case, to Refs. 45–47.

In order to reduce by the flows of H and L_z it is useful to rewrite G as

$$G = L_z^2 - 2R^2 - \frac{2}{\omega}(a^2\omega^2 - H)R + \frac{1}{\omega}X, \tag{9}$$

where

$$R := \frac{1}{\omega}(A_x + A_y), \tag{10}$$

$$X := \omega(L_x^2 + L_y^2) - 2A_z R. \tag{11}$$

The significance of this decomposition is that defining Y by

$$\{R, X\} = -2Y,$$

we find that the Poisson brackets between R, X, and Y are closed. Specifically, we have

$$\{R, Y\} = 2X \text{ and } \{X, Y\} = 8(H - \omega R)(\omega L_z^2 + HR - 2\omega R^2)$$

and (R, X, Y) form a closed Poisson algebra with the Casimir function

$$C = 4\omega^2(H - \omega R)^2(R^2 - L_z^2) - \omega^2(X^2 + Y^2) = 0. \tag{12}$$

Hence, this achieves reduction to a single degree of freedom with phase space given by the zero level set of the Casimir function C.

A systematic way to achieve this reduction uses invariant polynomials. This approach is moreover useful because it gives a classical analogue to creation and annihilation operators used in the quantization below. The flows generated by (H, L_z) define a T^2 action on the original phase space $T^*\mathbb{R}^3$. Since both H and L_z are quadratic and they satisfy $\{H, L_z\} = 0$, there is a linear symplectic transformation that diagonalises both H and L_z. It is given by

$$x = \frac{1}{\sqrt{2\omega}}(p_1 + p_2),\ y = \frac{1}{\sqrt{2\omega}}(q_1 - q_2),\ z = \frac{1}{\sqrt{\omega}}q_3,\ p_x = -\sqrt{\frac{\omega}{2}}(q_1 + q_2),\ p_y = \sqrt{\frac{\omega}{2}}(p_1 - p_2),\ p_z = \sqrt{\omega}p_3.$$

In the new complex coordinates $z_k = p_k + iq_k$, $k = 1, 2, 3$, we find

$$H = \frac{\omega}{2}(z_1\bar{z}_1 + z_2\bar{z}_2 + z_3\bar{z}_3), \quad L_z = \frac{1}{2}(z_1\bar{z}_1 - z_2\bar{z}_2).$$

Additional invariant polynomials are

$$R = \frac{1}{2}(z_1\bar{z}_1 + z_2\bar{z}_2), \quad X - iY = \omega z_1 z_2 \bar{z}_3^2.$$

These invariants are related by the syzygy $C = 0$ in Eq. (12) and satisfy $|L_z| \le R \le H/\omega$.

The surface $C = 0$ in the three-dimensional space (X, Y, R) can be viewed as the reduced phase space. It is rotationally symmetric about the R axis. Due to a singularity at $R = E/\omega$ and another singularity at $R = 0$ when $l_z = 0$, the reduced space is homeomorphic but not diffeomorphic to a two-dimensional sphere [see Fig. 4(a) and 4(b)]. The singularities of the reduced space result from nontrivial isotropy of the S^1 action of the flow of L_z. The singularity at $R = 0$ when $l_z = 0$ corresponds to a fixed point of the S^1 action, while the singularities at $R = E/\omega$ correspond to points with $\mathbb{Z}_2$ isotropy. $R = 0$ implies that the full energy is contained in the z degree of freedom and motion consists of oscillations along the z axis. The corresponding phase space points are fixed points of the S^1 action of the flow of L_z. The value of L_z is zero for this motion. For $R = E/\omega$, the energy is contained completely in the x and y degrees of freedom [see (10)], i.e., the motion takes place in the (x, y) plane. This includes also the motion along the circle of radius $(|l_z|/\omega)^{1/2}$ where the vector fields generated by L_z and G are parallel.

The dynamics on the reduced phase space is generated by G. As the system has only one degree of freedom, the solutions are given by the level sets of G restricted to $C = 0$. As G is independent of Y the surfaces of constant G are cylindrical in the space (X, Y, R). Given the rotational symmetry of the reduced phase space the intersections of $G = g$ and $C = 0$ can be studied in the slice $Y = 0$ (see Fig. 4). Two intersection points in the slice result in a topological circle. Under variation of the value of the level g, the two intersection points collide at a tangency or the singular point where $R = E/\omega$ corresponding to the maximal and minimal values of g for which there is an intersection, respectively. Both cases correspond to elliptic equilibrium points for the flow of G on the reduced space. For $l_z = 0$, one of the intersection points can be at the singular point where $R = 0$. From Eq. (9), we see that the corresponding value of g is 0. In this case, the topological circle is not smooth. Away from the singular point $R = 0$, the points on this curve correspond to circular orbits of the action of L_z giving together with the fixed point of the action L_z at $R = 0$ a pinched 2-torus where the pinch is a focus-focus singular point in the space reduced by the flow of H. Reconstructing the reduction by the flow of H results in the product of a pinched 2-torus and a circle in the original full phase space $T^*\mathbb{R}^3$.

The minimal value of G attained at the singular point $R = E/\omega$ can be obtained from Eq. (9) and gives again (6). The maximal value of G can be computed from the condition that ∇G and ∇C are dependent on $C = 0$, where ∇ is with respect to the coordinates on the reduced space (R, X, Y). Similarly to the computation of the maximal value of g for fixed E and l_z in Subsection III B this leads to a cubic equation. The critical energy at which the focus-focus singular point comes into existence corresponds to the collision of the tangency that gives the

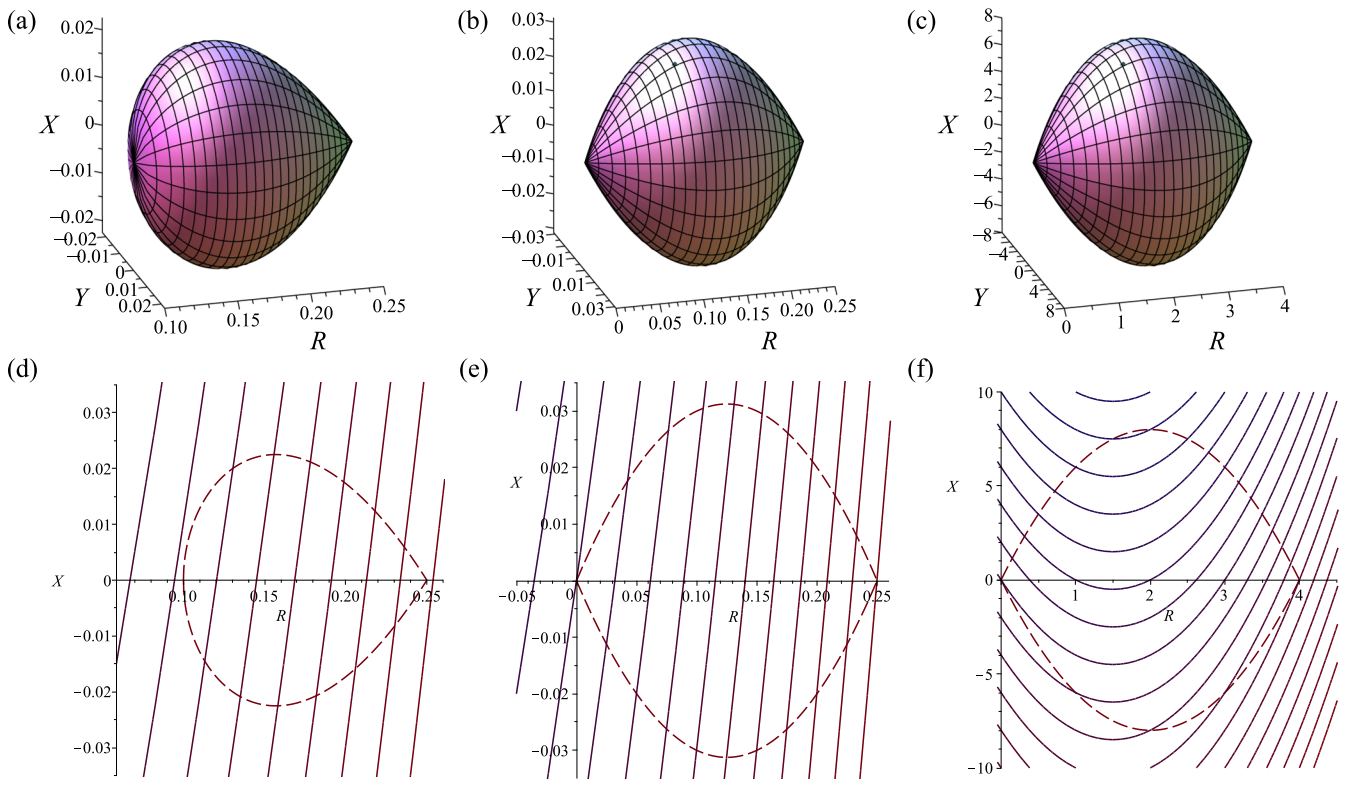

FIG. 4. Reduced space $C = 0$ for $E = 1/4$ and $l_z = 0.1$ (a), $E = 1/4$ and $l_z = 0$ (b), and $E = 4$ and $l_z = 0$ (c). The lower panels show the corresponding slices $Y = 0$ (dashed) and contours $G = g$ with increments $\Delta g = 0.05$ in (d) and (e) and $\Delta g = 2$ in (f). In all panels, $a = \omega = 1$.

maximal value of g with the singular point $R = 0$. As mentioned in Subsection III B, this corresponds to a Hamiltonian Hopf bifurcation. The critical energy can be computed from comparing the slope of the upper branch of the slice $Y = 0$ of $C = 0$ at $R = 0$ which is $2E$ with the slope of $G = 0$ at $R = 0$ which is $2a^2\omega^2 - 2E$. Equating the two gives the value $E = \frac{1}{2}\omega^2 a^2$ that we already found in Subsection III B.

D. Symplectic volume of the reduced phase space

It follows from the Duistermaat-Heckman Theorem[48] that the symplectic volume (area) of the reduced phase space defined by $C = 0$ has a piecewise linear dependence on the global action L_z. Indeed, introducing cylinder coordinates to parametrize the reduced phase space $C = 0$ as $X = f(R)\sin\theta$ and $Y = f(R)\cos\theta$, we see from $\{\theta, R\} = 2$ that the symplectic form on $C = 0$ is $\frac{1}{2}\, d\theta \wedge dR$. Integrating the symplectic form over the reduced space $C = 0$ gives the symplectic volume

$$\mathrm{Vol}_{E,l_z} = \frac{\pi}{\omega}(E - \omega|l_z|),$$

for fixed $E \geq \omega|l_z|$. It follows from Weyl's law that $\mathrm{Vol}_{E,l_z}/(2\pi\hbar) = (E - \omega|l_z|)/(2\hbar\omega)$ gives the mean number of quantum states for fixed E and l_z (see Ref. 49 for a recent review). Indeed inserting $E = \hbar\omega(n + 3/2)$ and $l_z = \hbar m$, we get $\mathrm{Vol}_{E,l_z}/(2\pi\hbar) = (n + 3/2 - |m|)/2$. Counting the exact number of states for fixed n and m which is most easily done using the separation with respect to spherical coordinates (see Introduction), we get $(n + 2 - |m|)/2$ if $n - |m|$ is even and $(n + 1 - |m|)/2$ if $n - |m|$ is odd. We see that Weyl's law is interpolating between the even and the odd case; see Fig. 5(a). Similar results relating the symplectic volume of the reduced phase space and the corresponding number of quantum states in specific physical systems have been obtained for systems of coupled angular momenta[50] and for the 1:1:2 resonant swing spring.[51]

The area under the graph of Vol_{E,l_z} as a function of l_z for fixed $E = \hbar\omega(n + 3/2)$ is $\pi\hbar^2(n + 3/2)^2$. Dividing by the product of $2\pi\hbar$ and $\hbar$ (which is the distance between two consecutive quantum angular momenta eigenvalues l_z) gives $(n + 3/2)^2/2$ which for $n \to \infty$ asymptotically agrees with the exact number of states $(n + 1)(n + 2)/2$; see Fig. 5(b).

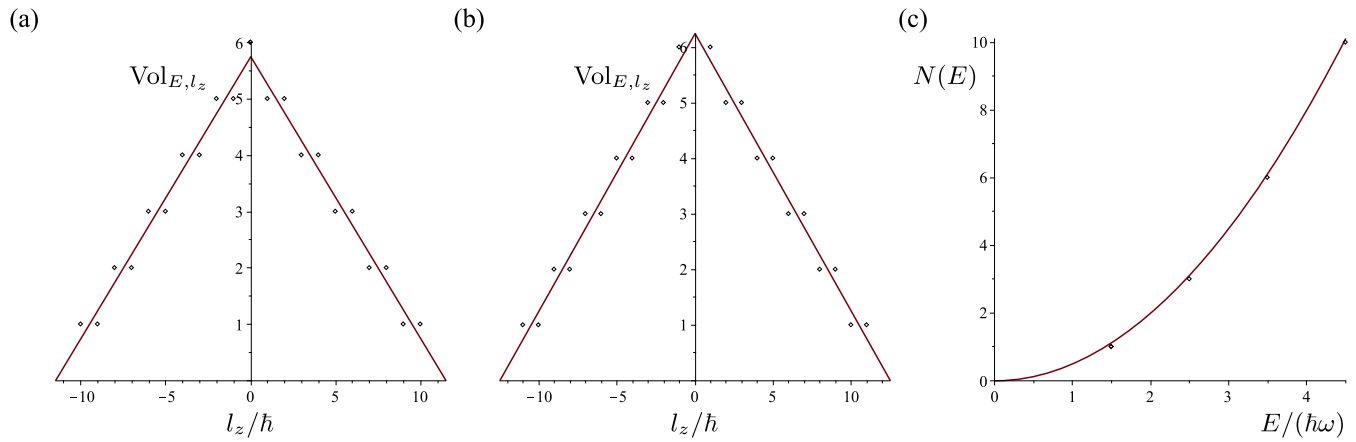

FIG. 5. Vol_{E,l_z} versus $m = l_z/\hbar$ for $E = \hbar\omega(n + 3/2)$ and corresponding exact number of states (dots) for the even integer $n = 10$ (a) and the odd integer $n = 11$ (b). (c) The area $N(E)$ under graphs of the form in (a) and (b) divided by $2\pi\hbar^2$ versus E and the corresponding exact number of states (dots) at energies of $\hbar\omega(n + 3/2)$.

E. The limiting cases $a \to 0$ and $a \to \infty$

From Eq. (3), we see that for $a \to 0$, the separation constant G becomes the squared total angular momentum, $\mathbf{L}^2 = L_x^2 + L_y^2 + L_z^2$. In the limit $a \to 0$, we thus obtain the Liouville integrable system given by $(H, L_z, |\mathbf{L}|^2)$ which corresponds to separation in spherical coordinates. Note that the $a \to \infty$ limit of prolate spheroidal coordinates corresponds to parabolic coordinates, where the harmonic oscillator is not separable. However, the scaled separation constant

$$\tilde{G} = -\frac{1}{a^2}G = 2(A_x + A_y) - \frac{1}{a^2}(L_x^2 + L_y^2 + L_z^2) \tag{13}$$

has the well defined limit $2(A_x + A_y)$ as $a \to \infty$. The limit $a \to \infty$ then leads to the Liouville integrable system $(H, L_z, 2(A_x + A_y))$. The standard separation in Cartesian coordinates leads to the integrable system (H, A_x, A_y).

The reduction by the flow of H gives as the reduced space the compact symplectic manifold $\mathbb{C}P^2$; see Sec. II. Then the map (A_x, A_y) associated with separation in Cartesian coordinates defines an effective toric action on $\mathbb{C}P^2$. The image of $\mathbb{C}P^2$ under (A_x, A_y) is therefore a

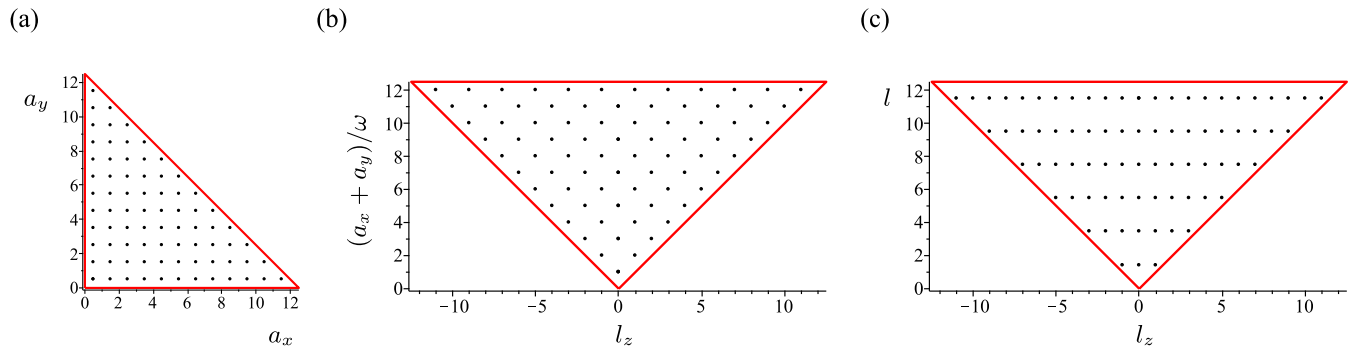

FIG. 6. The images of different maps of integrals $\mathbb{C}P^2 \to \mathbb{R}^2$ where $\mathbb{C}P^2$ is the energy level set of the harmonic oscillator reduced by the flow of the Hamiltonian H. (a) The map of integrals (A_x, A_y) associated with separation in Cartesian coordinates, where we denote the values of the functions A_k by a_k, $k = x, y$. The image is enclosed by the triangle with corners (0, 0), (0, E) and (E, 0). (b) The map of integrals $(L_z, \frac{1}{\omega}(A_x + A_y))$ associated with the limit ($a \to \infty$) when separating in prolate spheroidal coordinates. The image is enclosed by the triangle with corners (0, 0), (E/ω, E/ω) and ($-E/\omega$, E/ω). (c) The map of integrals (L_z, $|\mathbf{L}|$) associated with separation in spherical coordinates and the limit ($a \to 0$) in prolate spheroidal coordinates. Here l denotes the value of the function $|\mathbf{L}|$. The image is enclosed by the triangle with corners (0, 0), (E/ω, E/ω) and ($-E/\omega$, E/ω). The dots mark the joint spectrum of the corresponding quantum operators. The energy is chosen to be $E = \omega\hbar(n + 3/2)$ with $n = 11$. The values of $\hbar$ and ω are chosen as 1.

Delzant polygon which is a convex polygon with special properties;[52] see Fig. 6(a). Note that similar moment polytopes can also be defined for systems with monodromy.[53]

Similarly, the map $(L_z, \frac{1}{\omega}(A_x + A_y)) : \mathbb{C}P^2 \to \mathbb{R}^2$ associated with separation in prolate spheroidal coordinates in the limit $a \to \infty$ also defines a toric, non-effective, action and its image is the convex, non-Delzant, polygon shown in Fig. 6(b). We here have scaled the separation constant in such a way that the S^1 actions associated with the flows of L_z and $\frac{1}{\omega}(A_x + A_y)$ have the same period.

The image of the map $(L_z, |\mathbf{L}|) : \mathbb{C}P^2 \to \mathbb{R}^2$ associated with the limit $a \to 0$ and separation in spherical coordinates also gives the same polygon as in the previous case; see Fig. 6(c). However, whereas here L_z is a global S^1 action this is not the case for $|\mathbf{L}|$ whose Hamiltonian vector field is singular at points with $\mathbf{L} = 0$. Because of this singularity $(L_z, |\mathbf{L}|)$ is not the moment map of a global toric action. Whereas the image is a convex polygon the singularity manifests itself when considering the joint quantum spectrum of the operators associated with the classical constants of motion. Whereas these form rectangular lattices in Figs. 6(a) and 6(b) with lattice constants $\hbar$, this is not the case in Fig. 6(c) where the distance between consecutive lattice layers is not constant in the vertical direction.

IV. QUANTUM MONODROMY

In this section, we discuss the implications of the monodromy discussed in Sec. III on the joint spectrum defined by quantum operators $\hat{H}, \hat{L}_z, \hat{G}$. The quantum mechanical version of the isotropic oscillator is described by the operator

$$\hat{H} = -\frac{\hbar^2}{2}\nabla^2 + \frac{\omega^2}{2}(x^2 + y^2 + z^2).$$

In prolate spherical coordinates, the Schrödinger equation becomes

$$-\frac{\hbar^2}{2}\left\{\frac{1}{a^2(\xi^2-\eta^2)}\left[\frac{\partial}{\partial\xi}\left((\xi^2-1)\frac{\partial\Psi}{\partial\xi}\right) + \frac{\partial}{\partial\eta}\left((1-\eta^2)\frac{\partial\Psi}{\partial\eta}\right)\right] + \frac{1}{a^2(\xi^2-1)(1-\eta^2)}\frac{\partial^2\Psi}{\partial\phi^2}\right\} + \frac{\omega^2}{2}a^2(\xi^2+\eta^2-1)\Psi = E\Psi.$$

Separating the Schrödinger equation in prolate spheroidal coordinates works similarly to the classical case discussed in Sec. II. The separated equations for η and ξ are

$$-\hbar^2\frac{1}{1-s^2}\frac{d}{ds}\left[(1-s^2)\frac{d\psi}{ds}\right] = \frac{P(s)}{(1-s^2)^2}\psi, \tag{14}$$

where $P(s)$ is again the polynomial that we defined for the classical case in Eq. (5), with $l_z = \hbar m$. This is the spheroidal wave equation with an additional term proportional to ω^2 coming from the potential. For $|s| < 1$, it describes the angular coordinate η, and for $s > 1$ the radial coordinate ξ of spheroidal coordinates.

Analogously to the classical case the separation constant g corresponds to the eigenvalue of the operator

$$\hat{G} = \hat{L}_x^2 + \hat{L}_y^2 + \hat{L}_z^2 - 2a^2(\hat{A}_x + \hat{A}_y), \tag{15}$$

where for $k = x, y, z$, the $\hat{L}_k$ are the components of the standard angular momentum operator, and the $\hat{A}_k = -\frac{1}{2}\hbar^2\partial_k^2 + \frac{1}{2}\omega^2k^2$ are the Hamilton operators of one-dimensional harmonic oscillators.

A WKB ansatz shows that the joint spectrum of the quantum integrable system $(\hat{H}, \hat{L}_z, \hat{G})$ associated with the separation in prolate spheroidal coordinates can be computed semi-classically from a Bohr-Sommerfeld quantization of the actions according to $I_\phi = \frac{1}{2\pi}\oint p_\phi \, d\phi = \hbar m$, $I_\eta = \frac{1}{2\pi}\oint p_\eta \, d\eta = \hbar(n_\eta + \frac{1}{2})$ and $I_\xi = \frac{1}{2\pi}\oint p_\xi \, d\xi = \hbar(n_\xi + \frac{1}{2})$ with $m \in \mathbb{Z}$ and non-negative quantum numbers n_η and n_ξ. Using the calculus of residues it is straightforward to show that $E = I_\eta + I_\xi + |I_\phi|$. Taking the derivative with respect to l_z using $I_\phi = l_z$ shows that the actions I_η and I_ξ are not globally smooth functions of the constants of motion (E, g, l_z). This is an indication that the quantum numbers do not lead to a globally smooth labeling of the joint spectrum. We will see this in more detail below.

A. Confluent Heun equation

It is well known that the spheroidal wave equation can be transformed into the confluent Heun equation.[54] Adding the harmonic potential adds additional terms that dominate at infinity, and so a different transformation needs to be used to transform (14) into the Heun equation. We change the independent variable s in (14) to u by $s^2 = u$ and the dependent variable to y by $y(u) = \exp(a^2\omega u/(2\hbar))(1-u)^{-m/2}\psi(s)$ which leads to

$$y'' + \left(-\frac{a^2\omega}{\hbar} - \frac{m+1}{1-u} + \frac{1}{2u}\right)y' + Qy = 0,$$

where

$$Q = \frac{g - \hbar^2 m(m+1)}{4\hbar^2 u(1-u)} + \frac{a^2}{2\hbar^2}\left(\frac{\hbar(m+1)}{1-u} + \frac{E - \frac{1}{2}\hbar\omega}{u}\right).$$

This is a particular case of the confluent Heun equation, with regular singular points at 0 and 1, and an irregular singular point of rank 1 at infinity. Each regular singular point has one root of the indicial equation equal to zero, so we may look for a solution of the form $y(u) = \sum_k a_k u^k = \sum_k b_{2k} s^{2k}$. This leads to the three-term recursion relation for the coefficients

$$b_{k-2}A_{k-2} + b_k B_k - b_{k+2}\hbar^2(k+1)(k+2) = b_k(g + 2a^2E),$$

where k is an even integer and

$$A_{k-2} = 2a^2(E - \hbar\omega(m + k - \tfrac{1}{2})),$$
$$B_k = a^2\hbar\omega(2k+1) + \hbar^2(m+k)(m+k+1).$$

If we require that $y(u)$ is polynomial of degree d, we need to require that for $k = 2d + 2$ the coefficient A_{k-2} vanishes, and hence the quantisation condition

$$E = \hbar\omega\left(m + 2\,d + \tfrac{3}{2}\right),$$

with principal quantum number $n = m + 2d$ is found. Fixing E to some half-integer the spectrum of the tridiagonal matrix M obtained from the three-term recurrence relation determines the spectrum of $g + 2a^2E$. In the limit $a \to 0$, the spectrum becomes $n(n+1), \ldots, m(m+1)$. Note that fixing the energy and allowing all possible degrees d makes m change in steps of 2. Since m in fact changes in steps of 1 there must be additional solutions.

The regular singular point at $u = 0$ has another regular solution with leading power $\sqrt{u}$ = s, so that we make the Ansatz $y(u) = \sqrt{u}\sum_0 a_k u^k = \sum_0 b_{2k+1} s^{2k+1}$, which leads to an odd function in s. The same three-term recursion relation holds as above, except that now the index k is odd. For $a \to 0$, the spectrum is $n(n+1), \ldots, (m+1)(m+2)$, as before in steps of 2 in m.

We note that in the spherical limit $a \to 0$, the Heun equation reduces to the associated Laguerre equation with polynomial solutions $L^{l+1/2}_{(n-l)/2}(s^2)$ when $g = l(l+1)$.

B. Algebraic computation of the joint spectrum

Instead of starting from the spheroidal wave equation wave equation as illustrated in Subsection IV A, one can directly compute the joint spectrum algebraically by using creation and annihilation operators. As we will see this gives explicit expressions for the entries of a tri-diagonal matrix whose eigenvalues give the spectrum of $\hat{G}$ for fixed E and l.

Instead of the usual creation and annihilation operators of the harmonic oscillator we use operators that are written in the set of coordinates (z_1, z_2, z_3) introduced in Sec. III C. The transformation to the new coordinates diagonalises $\hat{L}_z$ and at the same time keeps $\hat{H}$ diagonal so that

$$\hat{H} = \hbar\omega(a_1^\dagger a_1 + a_2^\dagger a_2 + a_3^\dagger a_3 + \tfrac{3}{2}), \quad \hat{L}_z = \hbar(a_1^\dagger a_1 - a_2^\dagger a_2)$$

and the operator $\hat{R}$ corresponding to the classical R in Eq. (10) reads

$$\hat{R} = \hbar(a_1^\dagger a_1 + a_2^\dagger a_2 + 1).$$

The operator $\hat{X}$ corresponding to X in Eq. (11) is of higher degree, and thus care needs to be taken with the order of operators. The classical X can be written as $X = \frac{1}{2}\omega(z_1 z_2 \bar{z}_3^2 + \bar{z}_1 \bar{z}_2 z_3^2)$. We also need to preserve the relation (for operators!) $\omega\hat{L}^2 = \omega\hat{L}_z^2 + 2(\hat{H} - \omega\hat{R})\hat{R} + \hat{X}$, cf. Eq. (11), and this leads to

$$\hat{X} = 2\hbar^2\omega\left(a_1^\dagger a_2^\dagger a_3^2 + a_1 a_2 (a_3^\dagger)^2 - \frac{1}{2}\right).$$

With these expressions matrix elements can be computed. Denote a state with three quantum numbers associated with the creation and annihilation operators a_i and $a_i^\dagger$, $i = 1, 2, 3$, by $|k_1, k_2, k_3\rangle$, such that

$$\begin{aligned} a_1^\dagger|k_1,k_2,k_3\rangle &= \sqrt{n_1+1}|k_1+1,k_2,k_3\rangle,\\ a_1|k_1,k_2,k_3\rangle &= \sqrt{n_1}|k_1-1,k_2,k_3\rangle, \text{ for } k_1 \geq 1,\\ a_1|0,k_2,k_3\rangle &= 0 \end{aligned}$$

and similar relations for a_2 and a_3. This allows us to verify

$$\begin{aligned} \hat{H}|k_1,k_2,k_3\rangle &= \hbar\omega(k_1+k_2+k_3+\tfrac{3}{2})|k_1,k_2,k_3\rangle,\\ \hat{L}_z|k_1,k_2,k_3\rangle &= \hbar(k_1-k_2)|k_1,k_2,k_3\rangle. \end{aligned}$$

In terms of the quantum numbers (k_1, k_2, k_3), the principal and magnetic quantum numbers are $n = k_1 + k_2 + k_3$ and $m = k_1 - k_2$, respectively. The space of states with fixed n and fixed m is the span of the states of the form

$$|k\rangle := |k, k-m, n+m-2k\rangle, \quad \max(0,m) \leq k \leq \frac{1}{2}(n+m).$$

Now the non-zero matrix elements of

$$\hat{G} = \hat{\mathbf{L}}^2 - 2a^2\omega\hat{R} = \hat{L}_z^2 - 2\hat{R}^2 - \frac{2}{\omega}(a^2\omega^2 - \hat{H})\hat{R} + \frac{1}{\omega}\hat{X}$$

are given by

$$\begin{aligned} \langle k|\hat{G}|k\rangle &= 2\hbar a^2\omega(m-1-2k) + \hbar^2[m^2-1-2(m-1-2k)^2-(m-1-2k)(3+2n)]\\ &= 2\hbar a^2\omega(m-1-2k) - \hbar^2[m^2+2mn-2n-m+8k^2+2k-8km-4kn]\\ \langle k|\hat{G}|k+1\rangle &= 2\hbar^2\sqrt{(k+1)(k+1-m)(n-1+m-2k)(n+m-2k)}. \end{aligned}$$

The resulting joint spectrum of $(\hat{L}_z, \hat{G})$ for a fixed n is shown in Fig. 7 for a choice of parameters such that the energy E is above the threshold value $\frac{1}{2}\omega^2a^2$ for the occurrence of monodromy. As to be expected from the Bohr-Sommerfeld quantization of actions the spectrum locally has the structure of a regular grid. Globally, however, the lattice has a defect as can be seen from transporting a lattice cell along a loop that encircles the isolated critical value of the energy momentum map at the origin; see Refs. 17, 45, and 55.

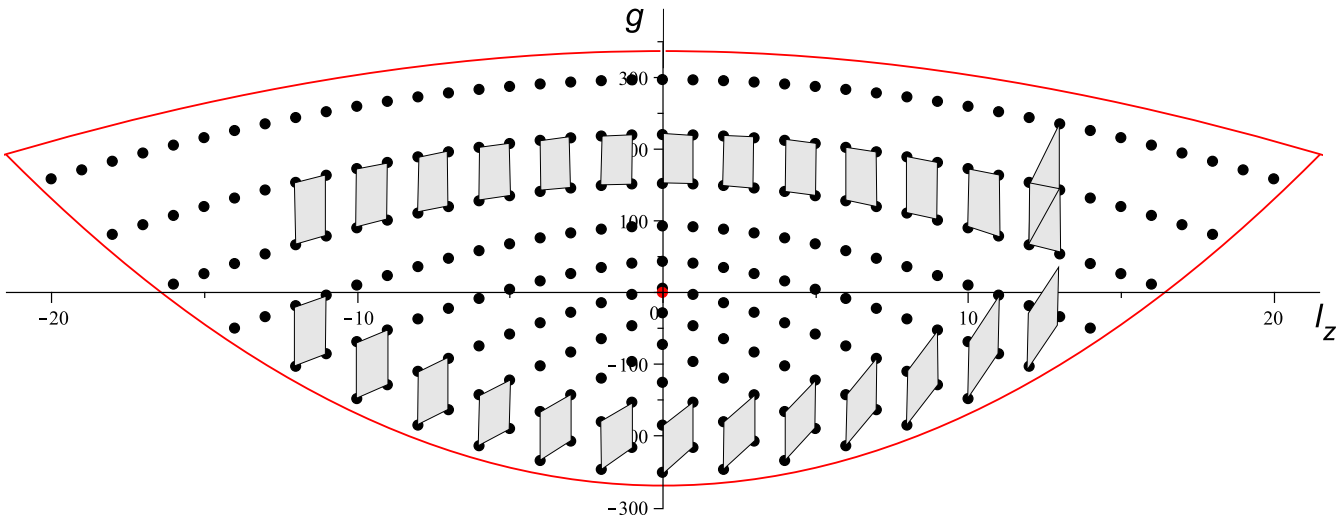

FIG. 7. Joint spectrum (l_z, g) of $(\hat{L}_z, \hat{G})$ (black dots) and classical critical values (red), for $n = 20$, $\omega = 1$, $\hbar = 1$, and $a = 3/2$. There are $(n + 1)(n + 2)/2$ joint states. The joint spectrum locally has a lattice structure which globally has a defect as can be seen from transporting a lattice cell around the isolated critical value at the origin.

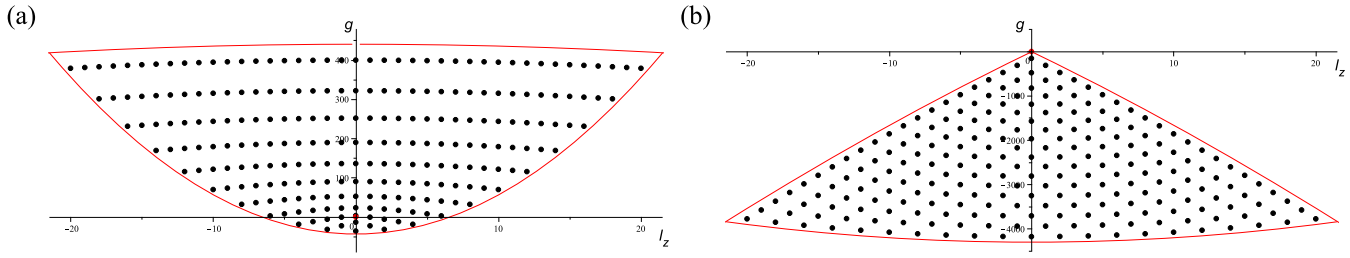

FIG. 8. Joint spectrum (l_z, g) of $(\hat{L}_z, \hat{G})$ (black dots) and classical critical values (red) for $a = 1$ (a) and $a = 10$ (b) and otherwise same parameters as in Fig. 7.

In Fig. 8, the joint spectrum of $(\hat{L}_z, \hat{G})$ is shown for fixed n and a small and large value of a, respectively. As discussed in Sec. III E, in the limits $a \to 0$ and $a \to \infty$ (and in the latter case changing to $\tilde{G} = -\frac{1}{a^2}G$) the images become the polygones shown in Fig. 6.

V. DISCUSSION

It is interesting to compare the two most important super-integrable systems, the Kepler problem and the harmonic oscillator, in the light of our analysis. The Kepler problem has symmetry group SO(4) and reduction by the Hamiltonian flow leads to a system on $S^2 \times S^2$.[38] The 3-dimensional harmonic oscillator has symmetry group $SU(3)$ and reduction by the Hamiltonian flow leads to a system on $\mathbb{C}P^2$.

Separation of both systems, the Kepler problem and the harmonic oscillator in 3 dimensions, in prolate spheroidal coordinates leads to Liouville integrable systems that are of toric type for sufficiently large a. Here, the technical meaning of toric type is that they are integrable systems with a global T^n action for n degrees of freedom, which implies that all singularities are of elliptic type. To a toric system is associated the image of the momentum map of the T^n action, and this is a Delzant polytope, a convex polytope with special properties.[52] The Delzant polytope for the T^2 action of the reduced Kepler system on $S^2 \times S^2$ is a square (take the limit $a \to \infty$ in Fig. 4 in Ref. 12) while the Delzant polytope for the T^2 action of the reduced harmonic oscillator on $\mathbb{C}P^2$ is an isosceles right triangle, see Fig. 6(a). It is remarkable that the two simplest such polytopes appear as reductions from the Kepler problem and from the harmonic oscillator. We note, however, that the harmonic oscillator as opposed to the Kepler problem does not separate in parabolic coordinates. This is related to the fact that for the separation of the Kepler problem in prolate spheroidal coordinates, the origin is in a focus point, while for the oscillator the origin is the midpoint between the foci.

For decreasing family parameter a, both systems become semi-toric[56,57] through a supercritical Hamiltonian Hopf bifurcation. It thus appears that the reduction of super-integrable systems by the flow of H leads to natural and important examples of toric and semi-toric systems on compact symplectic manifolds.

ACKNOWLEDGMENTS

We thank an anonymous referee for detailed comments that contributed to the presentation of this paper.

REFERENCES

[1] D. M. Fradkin, Am. J. Phys. **33**, 207 (1965).
[2] V. I. Arnold, *Mathematical Methods of Classical Mechanics*, Graduate Texts in Mathematics (Springer, Berlin, Heidelberg, New York, 1978), Vol. 60.
[3] F. Fassò, Acta Appl. Math. **87**, 93 (2005).
[4] N. N. Nehorošev, Trudy Moskov. Mat. Obšč. **26**, 181 (1972).
[5] A. S. Miščenko and A. T. Fomenko, Funct. Anal. Appl. **12**, 113 (1978).
[6] P. Dazord, T. Delzant *et al.*, J. Differ. Geom. **26**, 223 (1987).
[7] K. Schwarzschild, Sitz. Ber. Kgl. Preuss. Akad. d. Wiss. Berlin **1916**, 548.
[8] E. G. Kalnins, J. M. Kress, and W. Miller, Jr, J. Math. Phys. **47**, 043514 (2006).
[9] E. P. Wigner, *Group Theory and its Application to the Quantum Mechanics of Atomic Spectra* (Academic Press, New York, 1959) [translation by J. J. Griffin of E. P. Wigner, Gruppentheorie und ihre Anwendung auf die Quantenmechanik der Atomspektren (Vieweg, Braunschweig, 1931)].
[10] D. J. Griffiths, *Introduction to Quantum Mechanics*, 2nd ed. (Cambridge University Press, Cambridge, 2016).
[11] J. J. Duistermaat, Commun. Pure Appl. Math. **33**, 687 (1980).
[12] H. R. Dullin and H. Waalkens, Phys. Rev. Lett. **120**, 020507 (2018).
[13] H. Waalkens, H. R. Dullin, and P. H. Richter, Physica D **196**, 265 (2004).
[14] N. N. Nekhoroshev, D. A. Sadovskiĭ, and B. I. Zhilinskiĭ, Ann. Henri Poincaré **7**, 1099 (2006).
[15] D. Sadovskiĭ and B. Zhilinskiĭ, Ann. Phys. **322**, 164 (2007).

[16]B. Zhilinskií, "Monodromy and complexity of quantum systems," in *The Complexity of Dynamical Systems: A Multi-Disciplinary Perspective*, edited by J. Dubbeldam, K. Green, and D. Lenstra (John Wiley & Sons, 2011), pp. 159–181.
[17]R. H. Cushman and J. J. Duistermaat, Bull. Am. Math. Soc. **19**, 475 (1988).
[18]S. Vũ Ngọc, Commun. Pure Appl. Math. **53**, 143 (2000).
[19]D. A. Sadovskií and B. I. Zhilinskií, Phys. Lett. A **256**, 235 (1999).
[20]B. Zhilinskií, "Hamiltonian monodromy as lattice defect," in *Topology in Condensed Matter*, edited by M. I. Monastyrsky (Springer Berlin Heidelberg, Berlin, Heidelberg, 2006), pp. 165–186.
[21]R. H. Cushman, H. R. Dullin, A. Giacobbe, D. D. Holm, M. Joyeux, P. Lynch, D. A. Sadovskíi, and B. Zhilinskiíi, Phys. Rev. Lett. **93**, 024302 (2004).
[22]M. S. Child, "Quantum monodromy and molecular spectroscopy," in *Advances in Chemical Physics*, edited by S. A. Rice (John Wiley & Sons, 2008), pp. 39–94.
[23]E. Assémat, K. Efstathiou, M. Joyeux, and D. Sugny, Phys. Rev. Lett. **104**, 113002 (2010).
[24]R. H. Cushman and D. A. Sadovskií, Europhys. Lett. **47**, 1 (1999).
[25]K. Efstathiou, D. Sadovskií, and B. Zhilinskií, Proc. R. Soc. A **463**, 1771 (2007).
[26]P. Cejnar, M. Macek, S. Heinze, J. Jolie, and J. Dobeš, J. Phys. A: Math. Gen. **39**, L515 (2006).
[27]M. Caprio, P. Cejnar, and F. Iachello, Ann. Phys. **323**, 1106 (2008).
[28]H. R. Dullin and H. Waalkens, Phys. Rev. Lett. **101**, 070405 (2008).
[29]N. Martynchuk and H. Waalkens, Regular Chaotic Dyn. **21**, 697 (2016).
[30]N. Martynchuk, H. Dullin, K. Efstathiou, and H. Waalkens, Nonlinearity **32**(4), 1296–1326 (2019).
[31]D. Sugny, A. Picozzi, S. Lagrange, and H. R. Jauslin, Phys. Rev. Lett. **103**, 034102 (2009).
[32]C. Chen, M. Ivory, S. Aubin, and J. Delos, Phys. Rev. E **89**, 012919 (2014).
[33]N. C. Leung and M. Symington, J. Symplectic Geom. **8**, 143 (2010).
[34]M. Symington, in *Proceedings of Symposia in Pure Mathematics* (American Mathematical Society, 2003), Vol. 71, p. 51.
[35]I. N. Kozin, D. A. Sadovskií, and B. I. Zhilinskií, Spectrochim. Acta, Part A **61**, 2867 (2005).
[36]V. Lanchares, A. I. Pascual, J. Palacián, P. Yanguas, and J. P. Salas, Chaos **12**, 87 (2002).
[37]S. Ferrer and J. Gárate, "On perturbed 3D elliptic oscillators: A case of critical inclination in galactic dynamics," in *New Trends for Hamiltonian Systems and Celestial Mechanics*, edited by E. A. Lacomba and J. Llibre (World Scientific, Singapore, 1996), pp. 179–197.
[38]J. Moser, Commun. Pure Appl. Math. **23**, 609 (1970).
[39]K. Efstathiou and D. A. Sadovskií, Nonlinearity **17**, 415 (2004).
[40]C. A. Coulson and A. Joseph, Proc. Phys. Soc. **90**, 887 (1967).
[41]R. H. Cushman and L. M. Bates, *Global Aspects of Classical Integrable Systems* (Birkhäuser, Basel, Boston, Berlin, 1997).
[42]R. H. Cushman, S. Ferrer, and H. Hanßmann, Nonlinearity **12**, 389 (1999).
[43]S. Ferrer, J. Palacián, and P. Yanguas, J. Nonlinear Sci. **10**, 145 (2000).
[44]L. Michel and B. I. Zhilinskií, Phys. Rep. **341**, 173 (2001).
[45]R. H. Cushman and D. A. Sadovskií, Physica D **142**, 166 (2000).
[46]K. Efstathiou, in *Metamorphoses of Hamiltonian Systems with Symmetries*, Lecture Notes in Mathematics, edited by J.-M. Morel, F. Takens, and B. Teissier (Springer, Berlin, Heidelberg, New York, 2005) p. 149.
[47]K. Efstathiou and D. A. Sadovskií, Rev. Mod. Phys. **82**, 2099 (2010).
[48]J. J. Duistermaat and G. J. Heckman, Inventiones Math. **69**, 259 (1982).
[49]V. Ivrii, Bull. Math. Sci. **6**, 379 (2016).
[50]L. Grondin, D. A. Sadovskií, and B. I. Zhilinskií, Phys. Rev. A **65**, 012105 (2001).
[51]A. Giacobbe, R. H. Cushman, D. A. Sadovskií, and B. I. Zhilinskií, J. Math. Phys. **45**, 5076 (2004).
[52]T. Delzant, Bull. Soc. Math. France **116**, 315 (1988).
[53]S. Vũ Ngọc, Adv. Math. **208**, 909 (2007).
[54]DLMF, "NIST Digital Library of Mathematical Functions," http://dlmf.nist.gov/, Release 1.0.19 of 2018-06-22 (2018), F. W. J. Olver, A. B. Olde Daalhuis, D. W. Lozier, B. I. Schneider, R. F. Boisvert, C. W. Clark, B. R. Miller, and B. V. Saunders.
[55]D. A. Sadovskií and B. I. Zhilinskií, Phys. Lett. A **256**, 235 (1999).
[56]A. Pelayo and S. Vũ Ngọc, Inventiones Math. **177**, 571 (2009).
[57]K. Efstathiou and N. Martynchuk, J. Geom. Phys. **115**, 104 (2017), FDIS 2015: Finite Dimensional Integrable Systems in Geometry and Mathematical Physics.